Thermoring Basis for the PIP_2-Dependent Cold Switches in the TRPM8 Biothermometer

Running title: Digit codes for cold-gated TRPM8

Guangyu Wang [1,2]*

[1]Department of Physiology and Membrane Biology, University of California School of Medicine, Davis, CA, USA

[2]Department of Drug Research and Development, Institute of Biophysical Medico-chemistry, Reno, NV, USA

* Correspondence: gary.wang10@gmail.com

Abstract

The menthol sensor TRPM8 can also be activated by cold and thus serves as a biothermometer in a primary afferent sensory neuron for noxious cold detection. However, the underlying design maps are unknown. Here, a series of cold-sensitive factors, together with a recently developed grid thermodynamic model, were employed to cross-examine if the available 3D structures of closed and open mouse TRPM8 with or without Ca^{2+} and PIP_2 and cooling agents bound can be directly used for cold detection. The results demonstrated that noncovalent interactions as identified in those structures could form a systematic fluidic grid-like mesh network along the PIP_2-dependent gating pathway. While the biggest $Grid_{21}$ near the lower gate may serve as a cold switch with a matched threshold of 22 °C for PIP_2 binding, the biggest $Grid_{26}$ in the pore domain may act as another cold switch with a matched threshold 7 °C to stabilize the open state. Further, PIP_2-dependent channel opening upon a cold incubation could create a matched temperature sensitivity of -28. Finally, both gating states passed the test of the available cold-sensitive factors including pH. Therefore, the captured structures of closed and open TRPM8 at low temperature could be used for noxious cold detection. (200 words)

Keywords: grid thermodynamic model, lipid, noncovalent interaction, temperature sensitivity, thermoring, threshold, TRP channel.

1. INTRODUCTION

Transient receptor potential (TRP) melastatin-8 (TRPM8) is a Ca^{2+}-permeable ion channel with outwardly rectification. It serves as a polymodal sensor in response to both physical and chemical stimuli. The physical stimuli include voltage and cold while the chemical stimuli cover phosphatidylinositol-4, 5-biphosphate (PIP_2) and cooling agents such as menthol and its analogs WS-12 and icilin. [1-9] When heat decreases the menthol-evoked activity of TRPM8 or menthol increases the temperature threshold and the saturation temperature of rat TRPM8 (rTRPM8) from 22-26 °C and 8.2 °C to 30-32°C and 15.6°C, respectively, the same gating pathway seems to be shared. [1-2, 10-16] However, some menthol-sensitive residues such as Y745 and Y1005 in mouse TRPM8 (mTRPM8) are insensitive to cold, challenging the same gating pathway. [17] Although the high-resolution cryo-electron microscopy (cryo-EM) structures of closed and open mTRPM8 at 4 °C and 20 °C are available in the absence or presence of Ca^{2+}, PIP_2, and cooling agents such as allyl isothiocyanate (AITC) and cryosim-3 (C3), [18-19] the structural factor or motif for the specific PIP_2-dependent cold temperature threshold and sensitivity is still missing.

Recent studies have demonstrated that a biological macromolecular has a thermoring structure to govern its thermal stability and activity. The thermoring can be a DNA hairpin in a single poly-nucleotide chain or a topological grid in a systematic fluidic grid-like noncovalent interaction mesh network of a single polypeptide chain. [20-24] Such a biochemical or biophysical network can be characterized by a graph theory-based grid thermodynamic model. First, a melting temperature threshold (T_m) for thermal unfolding of the thermoring from the biggest grid to the smallest one is determined by its strength and size. Second, the grid-based systematic thermal instability (T_i) at a specific temperature is governed by the ratio of the total grid size to the total noncovalent interactions. Third, a structural thermo-sensitivity (Ω_{10}) is controlled by a change in the total grid sizes upon a change in the total noncovalent interactions within a 10 °C interval. Once three calculated parameters match the experimental values including the functional thermo-sensitivity (Q_{10}, the ratio of rates or open probabilities (P_o) of an ion channel measured 10 °C apart), the specific thermoring for the structural thermostability or the functional thermoactivity can be identified. [21-24] Following a success in deciphering the lipid-dependent heat response and sensitivity of the TRP vanilloid 1 (TRPV1) channel, [24] it is attractive to use this graphical method to examine a hypothesis that temperature-dependent systematic fluidic grid-like noncovalent interaction mesh networks as identified in the 3D structures of the TRPM8 channel can be

constrained as a thermoring structure from the biggest grid to the smallest one to control the PIP_2-dependent cold-sensing with a high sensitivity.

In this computational study, two biggest grids in stable closed and open mTRPM8 channels were first identified as cold switches with matched thresholds from a starting 21 °C to a saturating 7 °C for PIP_2-dependent channel opening at intracellular pH 8. [10] Furthermore, the calculated structural thermo-sensitivity ($\Omega_{10,}$ -28) between two gating states was consistent with the experimental functional value ($Q_{10,}$ -24-35). Finally, cold-sensitive factors including pH and PIP_2 and ambient temperature, together with the comparative systematic thermal instability, were also employed to cross-examine the structures of both open and closed states. [10] Taken together, these two stable structures of mTRPM8 could be directly used to achieve PIP_2-dependent cold sensing with a matched 10-degree temperature coefficient Q_{10}.[10, 25]

2. MATERIALS AND METHODS

2.1 Data mining resources

The systemic fluidic grid-like non-covalently interacting mesh networks of mTRPM8 were based on the high-resolution cryo-EM structural data of closed mTRPM8 at 4 °C with Ca^{2+} bound (PDB ID, 7WRB, model resolution= 3.0 Å) and without Ca^{2+} bound (PDB ID, 7WRA, model resolution= 2.9 Å), [18] and open mTRPM8 at 20 °C with Ca^{2+}, PIP_2, C3 and AITC bound (PDB ID, 8E4L, model resolution= 3.32 Å). [19] UCSF Chimera was used for the thermoring analyses.

2.2 The definition of the necessary gating pathway

PIP_2 is required for TRPM8 opening. [5-6, 9] The cryo-EM structure indicates that S4b, TRP domain, and pre-S1 form the active PIP_2 binding pocket. [19] The primary structural analysis showed that apo mTRPM8 at 4 °C (PDB ID, 7WRA) had a disordered segment between F1030 and F1045 in the C-terminal domain, and F1013 in the C-terminal domain formed a π-π interaction with F744 on S1. On the other hand, Q675 in the pre-S1 domain H-bonded with R998 in the TRP domain.[18] Hence, the segment from Q675 in the pre-S1 domain to F1015 in the TRP domain should be at least included as the necessary PIP_2-dependent gating pathway for the specific temperature threshold and sensitivity and the reasonable systematic thermal instability.

2.3 Preparation of the systematic fluidic noncovalent interaction mesh network maps

For the thermoring structural analyses of a systematic fluidic grid-like mesh network, all the potential stereo- or regio-selective inter-domain diagonal and intra-domain lateral non-covalent

interactions such as salt/metal bridges and π interactions and H-bonds along the PIP_2-dependent gating pathway in closed or open mTRPM8 were filtered and geometrically mapped as described previously (Table S1-3). [21-24] The grid size was constrained as the minimal number of the total side chains of residues in protein or atoms in the bound lipid that did not engage in any non-covalent interaction in a grid. The Floyd-Warshall algorithm was used for the size constraint. [26] In this way, both shortest direct and reverse paths between two ends of a noncovalent interaction were available. For example, in the grid-like biochemical reaction mesh network of Fig.1A, a direct path length from W798 to H845 was zero because there was a π–π interaction between them. However, there was another shortest reverse path from H845 to the segment ^{844}IL^{843}, R842, E782, Y793 and back to W798 via two H-bonds and one π interaction. Because the segment between R842 and H845 in the grid had two residues not to participate in any non-covalent interaction, the grid size was 2. After each non-covalent interaction was tracked by a constrained grid size and the uncommon sizes were marked in black, a grid with an x-residue or atom size was denoted as $Grid_x$, and the total non-covalent interactions and grid sizes along the PIP_2-dependent gating pathway of one subunit were calculated and shown in black and cyan circles beside the mesh network map, respectively, for the calculation of the systematic thermal instability (T_i) and the defined structural thermo-sensitivity (Ω_{10}).

2.4 Equations

For a DNA hairpin thermo-sensor to have a 20-base loop and two G-C base pairs in the stem, a start control melting temperature threshold (T_m) to initiate thermal unfolding of the hairpin loop is 34 °C. Once an additional G-C base pair or five additional bases are added in the hairpin, the T_m can be increased by 10 °C. [20] Similarly, when a single polypeptide chain carries out rate-limiting thermal unfolding of the thermorings from the biggest grid to the smallest one, the T_m of thermal unfolding of the given grid along the PIP_2-dependent gating pathway was in turn calculated by using the following equation as described and examined previously: [21-24]

$$T_m\ (°C) = 34 + (n - 2) \times 10 + (20 - S_{max}) \times 2 \qquad (1)$$

where, n is the total number of the grid size-controlled simple H-bonds equivalent to non-covalent interactions in the given grid, and S_{max} is the size of the given grid. In this regard, either a decrease in the grid size or an increase in equivalent H-bonds can raise the grid's heat capacity.

On the other hand, the T_m of the DNA hairpin can be always increased by the more G-C base pairs in the stem or the shorter poly-A loop. [20] Thus, in either gating state, the systematic

thermal instability (T_i) along the PIP_2-dependent gating pathway was defined using the following equation as described and examined previously: [21-24]

$$T_i = S/N \quad (2)$$

where, S is the total grid sizes along the PIP_2-dependent gating pathway of one subunit in a given gating state; N is the total non-covalent interactions along the same PIP_2-dependent gating pathway of one subunit in the same gating state. In this way, the lower the T_i, the less the conformational entropy in the system.

In a temperature range ΔT, for an enthalpy-driven channel gating transition from a fully closed state to a fully open state, if the chemical potential of a grid is theoretically defined as the maximal potential for equivalent residues in the grid to form the tightest β-hairpin with the smallest loop via paired non-covalent interactions, [27] the grid-based structural thermo-sensitivity ($\Omega_{\Delta T}$) of a single ion channel can be defined and calculated using the following equations:

$$\Omega_{\Delta T} = [(S_c - S_o)E/2]^{(Hc/Ho)} = [(S_c - S_o)E/2]^{[(ENc)/(ENo)]} = [(S_c - S_o)E/2]^{(Nc/No)} \quad (3)$$

where, along the same PIP_2-dependent gating pathway of one subunit, N_c and N_o are the total non-covalent interactions, S_c and S_o are the total grid sizes, and H_c and H_o are the total enthalpy included in non-covalent interactions in the closed and open states, respectively. E is the energy strength of a non-covalent interaction in a range of 0.5-3 kJ/mol. Usually, E is 1 kJ/mol. [28] Thus, $\Omega_{\Delta T}$ actually mirrors a thermo-evoked change in the total chemical potential of grids upon a thermo-evoked change in the total enthalpy included in non-covalent interactions from a closed state to an open state along the same PIP_2-dependent gating pathway of one subunit.

When ΔT=10 °C, Ω_{10} could be comparable to the functional thermo-sensitivity (Q_{10}) of a single ion channel. Q_{10} during thermal activation was calculated using the following equations:

$$Q_{10} = -(X_1/X_2)^{10/(T2-T1)} \quad (4)$$

where, X_1 and X_2 are open probability (P_o) values or reaction rates of mTRPM8 obtained at temperatures T1 and T2 (measured in kelvin), respectively.

3. RESULTS

3.1 Identification of a cold switch in Ca^{2+}-free mTRPM8

For a given PIP_2-dependent gating pathway from Q675 in the pre-S1 domain to F1015 in the TRP domain of apo mTRPM8 at 4 °C and pH 8, if a disulfide bond between C929 and C940 was disrupted,[18] fourteen H-bonds, two salt bridges and thirty-six π interactions would shape a

systematic fluidic grid-like mesh network (Fig. 1A). When the total noncovalent interactions and grids size were 52 and 113, respectively (Fig. 1A, Table S1). the grid-based systematic thermal instability (T_i) was 2.17 (Table 1).

Table 1 New parameters of the TRPM8 bio-thermometer based on the grid thermodynamic model at pH 8

Construct	**mTRPM8**		
PDB ID	8E4L	7WRB	7WRA
Ca^{2+}	bound	bound	free
PIP_2	bound	free	free
Sampling temperature, °C	**20**	**4**	**4**
Gating state	open	inactivated	closed
Name of the biggest grid	$Grid_{26}$	$Grid_{21}$	$Grid_{21}$
Biggest grid size (S_{max})	26	21	21
Equivalent H-bonds in S_{max}	0.5	1.0	1.0
Total non-covalent interactions	32	54	52
Total grid sizes, a.a./atoms	97	107	113
Systematic thermal instability (T_i)	3.03	1.98	2.17
Calculated T_m, °C	**7**	**22**	**22**
Measured threshold T_{th}, °C	**8.2**	**21**	**21**
Calculated $\Omega_{10,\ min}$ at E=0.5 kJ/mol		-4.70	-9.19
Calculated $\Omega_{10,\ mean}$ at E=1.0 kJ/mol		**-15.2**	**-27.9**
Calculated $\Omega_{10,\ max}$ at E=3.0 kJ/mol		-97.2	-162
Measured Q_{10}			**-23.8 to -35**
Ref. for measured **T_{th} and Q_{10}**	[1]	**[10,** 29**]**	**[**10, 25**]**

Of special note, the biggest $Grid_{21}$ was outstanding in the S4-S5 linker/S5/S6/TRP interfaces. It had a 21-residue size via the shortest path from P855 to D866, T982, W994, and back to P855 (Fig.1B-C). When 1.0 equivalent H-bond sealed this biggest $Grid_{21}$ to hold the P855-W994 π interaction in the S4-S5 linker/TRP interface (Fig. 1B-C), the calculated melting temperature threshold (T_m) was 22 °C, which was close to the experimental threshold 21 °C at pH

8 to initiate cold activation of TRPM8. [10] Thereafter, the biggest $Grid_{21}$ may act as a start cold switch in Ca^{2+}-free TRPM8 for correct PIP_2 binding at an optimal temperature 22 °C.

3.2 Identification of a cold switch in Ca^{2+}-bound mTRPM8

It has been reported that Ca^{2+} binding cannot change the temperature threshold for cold-evoked activation of TRPM8.[29] Therefore, it is necessary to test if Ca^{2+} binding affect the cold switch. When the Ca^{2+} bridge linked E782, Q795, N799 and D802 together, only small changes were observed at 4 °C and pH 8. For example, in the voltage-sensor-like domain (VSLD), the Q785-Y793 H-bond was disrupted but the Y772-I813 π interaction was added. In the pore domain, the R885-D918 H-bond was broken while the D925-H928 H-bond appeared. When the total noncovalent interactions and grid sizes were changed from 52 and 113 to 54 and 107, respectively (Fig. 2A, Table S2), the systematic thermal instability (T_i) was significantly decreased from 2.17 to 1.98 (Table 1). In any way, the biggest $Grid_{21}$ was not affected (Fig. 2). Thereby, the calculated threshold was still 22 °C, which was independent of Ca^{2+} binding (Table 1). In other words, the same cold switch was shared in the presence of Ca^{2+}.

3.3. Identification of another cold switch in PIP_2-bound mTRPM8 for channel opening

In the presence of not only Ca^{2+} but also PIP_2, C3, and AITC at 4 °C and pH 8, mTRPM8 was open with several changes in the systematic fluidic grid-like noncovalent interaction mesh network (Fig. 3A). First, C3 and AITC were bound against Y745 and W798 in the VSLD, respectively. [19] However, these two cooling agonists did not link any two residues together via noncovalent interactions (Fig. 3A). Second, PIP_2 was bound to R688 in the pre-S1 domain, R851 in the S4-S5 linker, and R998 in the TRP domain, forming a $Grid_7$ (Fig. 3B). Third, along with the PIP_2 binding, the gating $Grid_8$ was born with an 8-residue size via the shortest path from H845 to R851, W994, R998, Y999, F1000, E1004 and back to H845 (Fig. 3A-B). Fourth, when most of noncovalent interactions were maintained in the S5/S6 interface but disconnected in the outer pore loop (Figs. 2A & 3A), the biggest $Grid_{19}$ was primarily shown in the outer pore loop with a 19-residue size via the shortest path from R885 to Y905 and back to R885 to control the weak R885-Y905 cation-π interaction (Fig. 3A, 3D). When 0.5 equivalent H-bond sealed this $Grid_{19}$, the calculated T_m was about 21 °C. Therefore, it is reasonable that this bridge was present at 20 °C. [19] Once this R885-Y905 π interaction was replaced with the F874-Y908 one at 7 °C, the biggest $Grid_{26}$ would stabilize the open state via the shortest path from F874, W877, F881, Y908 and back to F874 (Fig. 3C-D). In that case, the total noncovalent interactions and grids size were 32 and 97,

respectively (Fig. 3A, Table S3). Thus, the grid-based systematic thermal instability (T_i) was 3.03 (Table 1). When this open state was used as a control, the calculated mean Ω_{10} for Ca^{2+}-free mTRPM8 was -27.9, which was close to the experimental Q_{10} range from -23.8 to -35 (Table 1). [10, 25] When Ca^{2+} was bound, the predicted mean Ω_{10} of 15.2 was in agreement with the desensitization role of Ca^{2+}. [4, 30]

3.4 Cross-examination of the cold switch in open mTRPM8

If the gating $Grid_8$ is required for mTRPM8 opening (Fig.4A), the cold effecacy should not be affected by some mutations. First, the H845A mutation has been reported not to affect the cold activation. [7] Thus, it is needed to examine if there is an alternative interaction of E1004 with a nearby residue. The rotamer simulation showed that R842 could still form a salt bridge with E1004 in the H845A mutant (Fig. 4B). Second, intracellular pH 6 has been reported to suppress responses to cold stimulation but not to affect responses to menthol. [10] Hence, it is also required to test if protonation of H835 at pH 6 can disassociate this gating $Grid_8$. The rotamer simulation indicated that protonated H835 still fomed a cation-π interaction with nearby W798 but failed to keep the H-bond with E1004. On the other hand, owing to an electronic interaction, positively charged R842 was far away from protonated H845 but close to the negatively charged residue D802. In this case, R842 could not form a salt bridge with E1004, either (Fig.4C). Thereafter, acidic pH 6 could disrupt this gating $Grid_8$, preventing mTRPM8 opening.

4. DISCUSSION

In this computational study, two cold switches were identified in the systemic fluidic grid-like non-covalently interacting mesh networks of mTRPM8. One was the biggest $Grid_{21}$ in the S4-S5 linker/S5/S6/TRP interfaces and the other was the biggest $Grid_{26}$ in the pore domain. When 1.0 equivalent H-bonds sealed the first with 21-residue size, the calculated 22 °C matched the experimental value 21 °C to favor correct PIP_2 binding for channel opening. On the other hand, once the temperature was further decreased to 7 °C, the open state could be stabilized by the second switch with a 26-residue size (Fig. 5). Further, the calculated structural temperature sensitivity (-28) matched the functional one (-23.8 to -35) between the stable PIP_2-free closed state and the stable PIP_2-bound open state. Therefore, these two cryo-EM structures could be used for noxious cold detection in a PIP_2-dependent manner. Like two classes of lipid-independent fructose

aldolases for the cycle reactions and lipid-dependent TRPV1 for heat-sensing, [21-24] the mTRPM8 activity also needed a flexible active site against rigid anchors for cold-sensing.

4.1 The thermo-stable S5-S6 interface was necessary for the active selectivity filter and the intact lower S6 gate

Although the outer pore loop was structured in the closed state but flexible in the open state, some noncovalent interactions in the pore domain were highly conserved in both closed and open states (Figs. 1A, 2A, 3A; Tables S1-S3). Because Y908 is close to the selectivity filter,[18-19] the highly conserved F874-Y908 and F881-Y963 π interactions may play an important role in keeping an active selectivity filter. On the other hand, since L975 is close to the lower S6 gate, the highly conserved D866-T982 H-bond and the F870-L975 π interaction may also be required as a stable anchor for the active lower S6 gate. In consonance with this proposal, D866, T982, F870, L975 were highly conserved in thermosensitive TRPV1-4 and TRPM2-5. [19, 31] The equivalent T680A mutation (T982 in mTRPM8) has been reported to suppress heat activation of TRPV3, [32] and the Y981F mutation in rTRPM8 is not functional. [33] Further, a loss of the D866-T982 H-bond also results in non-conducting TRPM8 even if PIP_2 has been bound. [19, 34] In contrast, the Y981K/E mutation destabilizes the lower gate, rendering rTRPM8 constitutively active. [33]

4.2 The thermostable pre-S1/TRP interface was needed for stimulatory PIP_2 binding

The W682-F735/F738 and Y683-F735 and F738-Y1005 π interaction network was also higly conserved in the pre-S1/TRP interface in both closed and open states (Figs. 1A, 2A & 3A; Tables S1-S2). These residues are also conserved in different species of TRPM8. [18-19] Thus, such a network may also serve as a thermo-stable anchor in favor of optimal PIP_2 binding for channel opening. In direct line with this notion, the disruption of this π interaction network by cholesterol hemisuccinate (CHS) also inactivates TRPM8. [30]

4.3 The flexible TRP domain was required for channel gating with tunable thresholds

The TRP domain interacts with not only the pre-S1 domain but also the VSLD and the S4-S5 linker and thus takes a pivotal role in channel gating. [18-19] The biggest $Grid_{21}$ may keep the intact pore domain below a matched threshold of 21 °C via the P855-W994 π interaction in favor of optimal PIP_2 binding (Figs. 1A & 2A). Once PIP_2 linked R851 in the S4-S5 linker and R688 in the pre-S1 domain and R988 in the TRP domain together, such a π bridge was replaced with the R851-D991 and H845-E1004 H-bonds for channel opening (Figs. 3-4). That may be why the R851A mutation results in a loss of function. [7]

In contrast, for pH-independent mTRPM8 activation by either the (-)-menthol dimer with head-to-head or the (+)-menthol dimer with head-to-tail, a "gas pedal" Y1005 is required for the TRP domain to be pushed away from the S6 bundle crossing gate against anchors L843 and I846 on S4 and Y745 on S1. [10, 35] In agreement with this proposal, when the pre-determined ambient temperature is increased from 30 °C to 40 °C, the nearby D781-R1008 salt bridge may induce the formation of the biggest $Grid_{14}$. When 0.5 equivalent H-bond sealed it via the shortest path from D781 to R784, Q785, Y793, N799, W798, H845, P855, W994, R998, Y999, F1000, E1004, R1008 and back to D781, the calculated T_m was about 31°C (Figs. 1A & 2A), which was close to the experimental value 30-34 °C at physiological pH 7.4, [1, 2, 10, 29] Once the R1008Q mutation broke this putative salt bridge, the similar threshold around 23 °C would be available at both pre-determined 30 °C and 40 °C at pH 7.4 [29]

On the other hand, protonation of H845 at acidic pH6 may change the H845-W798 π-π interaction to a cation-π interaction (Fig. 4C), weakening the P855-W994 π interaction allosterically for a decreased threshold. [10] Therefore, the biggest $Grid_{21}$ may favor correct PIP_2 binding at tunable 22-27 °C for channel opening at intracellular pH 8-7.4. [1, 2, 10, 18-19, 29, 33]

4.4 The flexible outer pore loop was necessary for TRPM8 opening with the high temperature sensitivity

Previous chimera study between mTRPM8 and chicken TRPM8 (cTRPM8) showed that the outer pore loop is thermosensitive. [36] In direct line with this notion, most of noncovalent interactions in the outer pore loop in the closed state were disconnected in the open state so that the systematic thermal instability (T_i) ascended from 2.17 to 3.03 upon PIP_2 binding. In this case, although mTRPM8 opening was initially enthalpy-driven ($\Delta H<0$), the increase in the systematic thermal instability (T_i) may facilitate the open state and the higher temperature sensitivity of -28 (Table 1).[10, 25] As Ca^{2+} binding decreased Ω_{10} from -28 to -15.2 (Table 1), it is reasonable that Ca^{2+} can desensitize cold-evoked TRPM8 activity.[4, 30]

5. CLOSING REMARK

The TRPM8 channel can be activated by both cold and cooling agents such as menthol and its analog WS-12 and icilin. This computational study demonstrated that both physical and chemical stimuli may share the similar gating pathway. Although Ca^{2+} binding was not necessary, PIP_2 was required to induce the stimulatory interaction between the voltage sensor and the TRP

domain. While the biggest $Grid_{21}$ on one side of the lower gate may favor PIP_2-dependent channel opening at a start threshold 22 °C, the biggest $Grid_{26}$ on the other side may stabilize the open state at temperature as low as 7 °C. Accordingly, this study may provide important clues as to how the TRPM8 biothermometer uses the thermorings from the biggest grid to the smallest one to achieve noxious cold detection with specific matched temperature thresholds and sensitivity.

Conventions and Abbreviations: AITC, allyl isothiocyanate; CHS, cholesterol hemisuccinate; C3, cryosim-3 or 1-diisopropylphosphorylnonane; cryo-EM, cryo-electron microscopy; PIP_2, phosphatidylinositol-4,5-bisphosphate; TRP, transient receptor potential; TRPM8, TRP melastatin-8; cTRPM8, chicken TRPM8; mTRPM8, mouse TRPM8; rTRPM8, rat TRPM8; VSLD, voltage-sensor-like domain

Acknowledgements

The author's own studies cited in this article were supported by the American Heart Association Grant (10SDG4120011 to GW), National Institute of Health Research Grant 2R56DK056796-10, and Cystic Fibrosis Foundation grant (DAWSON0210).

Author contributions

G. W. wrote the main manuscript text, prepared table 1 and figures 1-5 and tables S1-S3, and reviewed the whole manuscript and the Supplemental Information.

Conflict of Interest: The author declares no conflict of interest.

Data Availability Section: All data generated or analysed during this study are included in this published article.

References

1. D. D. McKemy, W. M. Neuhausser, D. Julius. Identification of a cold receptor reveals a general role for TRP channels in thermosensation. *Nature* 2002, **416,** 52-58.
2. A. M. Peier, A. Moqrich, A. C. Hergarden, A. J. Reeve, D. A. Andersson, G. M. Story, T. J. Earley, I. Dragoni, P. McIntyre, S. Bevan, A. Patapoutian. A TRP channel that senses cold stimuli and menthol. *Cell* 2002, **108,** 705-715.
3. G. Reid, A. Babes, F. Pluteanu. A cold- and menthol-activated current in rat dorsal root ganglion neurones:properties and role in cold transduction. *J Physiol (Lond)*, 2002, **545,** 595-614.
4. H. H. Chuang, W. M. Neuhausser, D. Julius, The super-cooling agent icilin reveals a mechanism of coincidence detection by a temperature-sensitive TRP channel. *Neuron*, 2004, **43,** 859-869.
5. T. Rohacs, C. M. B. Lopes, I. Michailidis, D. E. Logothetis. PI(4,5)P2 regulates the activation and desensitization of TRPM8 channels through the TRP domain. *Nat Neurosci.* 2005, **8,** 626-634.
6. B. Liu, F. Qin. Functional control of cold- and menthol-sensitive TRPM8 ion channels by phosphatidylinositol 4, 5-bisphosphate. *J Neurosci*. 2005, **25,** 1674-1681.
7. T. Voets, G. Owsianik, A. Janssens, K. Talavera, B. Nilius. TRPM8 voltage sensor mutants reveal a mechanism for integrating thermal and chemical stimuli. *Nat Chem Biol.* 2007, **3,** 174-182
8. M. Bodding, U. Wissenbach, V. Flockerzi. Characterisation of TRPM8 as a pharmacophore receptor. *Cell Calcium* 2007, **42,** 618-628.
9. E. Zakharian, C. Cao, T. Rohacs. Gating of transient receptor potential melastatin 8 (TRPM8) channels activated by cold and chemical agonists in planar lipid bilayers. *J Neurosci.* 2010, **30,** 12526-12534.
10. D. A. Andersson, H. W. Chase, S. Bevan. TRPM8 activation by menthol, icilin, and cold is differentially modulated by intracellular pH. *J Neurosci*, 2004, **24,** 5364-5369.
11. T. Voets, G. Droogmans, U. Wissenbach, A. Janssens, V. Flockerzi, B. Nilius. The principle of temperature-dependent gating in cold- and heat-sensitive TRP channels. *Nature* 2004, **430,** 748-754.

12. D. M. Bautista, J. Siemens, J. M. Glazer, P. R. Tsuruda, A.I. Basbaum, C. L. Stucky, S. E. Jordt, D. Julius. The menthol receptor TRPM8 is the principal detector of environmental cold. *Nature* 2007, **448,** 204-208.
13. R. W. Colburn, M. L. Lubin, D. J. Stone Jr., Y. Wang, D. Lawrence, M. R. D'Andrea, M. R. Brandt, Y. Liu, C. M. Flores, N. Qin. Attenuated cold sensitivity in TRPM8 null mice. *Neuron* 2007, **54,** 379-386.
14. A. Dhaka, A. N. Murray, J. Mathur, T. J. Earley, M. J. Petrus, A. Patapoutian. TRPM8 is required for cold sensation in mice. *Neuron* 2007, **54,** 371-378.
15. W. M. Knowlton, A. Bifolck-Fisher, D. M. Bautista, D. D. McKemy. TRPM8, but not TRPA1, is required for neural and behavioral responses to acute noxious cold temperatures and cold-mimetics in vivo. *Pain,* 2010, **150,** 340-350.
16. S. Wang, J. Lee, J. Y. Ro, M. K. Chung. Warmth suppresses and desensitizes damage-sensing ion channel TRPA1. *Mol Pain*. 2012, **8,** 22.
17. M. Bandell, A. E. Dubin, M. J. Petrus, A. Orth, J. Mathur, S. W. Hwang, A. High-throughput random mutagenesis screen reveals TRPM8 residues specifically required for activation by menthol. *Nat. Neurosci*. 2006, **9,** 493-500.
18. C. Zhao, Y. Xie, L. Xu, F. Ye, X. Xu, W. Yang, F. Yang, J. Guo. Structures of a mammalian TRPM8 in closed state. *Nat Commun*. 2022, **13,** 3113.
19. Y. Yin, F. Zhang, S. Feng, K. J. Butay, M. J. Borgnia, W. Im, S. Y. Lee.. Activation mechanism of the mouse cold-sensing TRPM8 channel by cooling agonist and PIP_2. *Science,* 2022, **378,** eadd1268.
20. Jonstrup AT, Fredsøe J, Andersen AH. DNA hairpins as temperature switches, thermometers and ionic detectors. Sensors. 2013, **13,** 5937-5944. doi: 10.3390/s130505937.
21. G. Wang. The network basis for the structural thermostability and the functional thermoactivity of aldolase B. *Molecules.* 2023, **28,** 1850.
22. G. Wang. Network basis for the heat-adapted structural thermostability of bacterial class II fructose bisphosphate aldolase. *ACS Omega.* 2023, **8,** 17731–17739.
23. G. Wang. Thermal ring-based heat switches in hyperthermophilic class II bacterial fructose aldolase. ACS Omega, 2023, **8,** 27, 24624–24634.
24. G. Wang. Thermoring-Based Heat Activation Switches in the TRPV1 Biothermometer. Int. J. Biol. Macromol. 2023 (in press). https://doi.org/10.1016/j.ijbiomac.2023.125915

25. S. Brauchi, P. Orio, R. Latorre. Clues to understanding cold sensation: Thermodynamics and electrophysiological analysis of the cold receptor TRPM8. *Proc. Natl. Acad. Sci.USA.*, 2004, **101,** 15494–15499.
26. R.W. Floyd. Algorithm-97 - Shortest Path. *Commun Acm* 1962, **5,** 345–345.
27. S. E. Kiehna, M. L. Waters. Sequence dependence of β-hairpin structure: Comparison of a salt bridge and an aromatic interaction. *Protein Science* 2003, **12,** 2657-2667.
28. A. J. Neel, M. J. Hilton, M. S. Sigman, F. D. Toste. Exploiting non-covalent π interactions for catalyst design. Nature. 2017, **543,**.637-645.
29. F. Fujita, K. Uchida, M. Takaishi, T. Sokabe, M. Tominaga. Ambient temperature affects the temperature threshold for TRPM8 activation through interaction of phosphatidylinositol 4, 5-bisphosphate. *J Neurosci*. 2013, **33,** 6154-6159.
30. M. M. Diver, Y. Cheng, D. Julius. Structural insights into TRPM8 inhibition and desensitization. *Science* 2019, **365,** 1434-1440.
31. K. D. Nadezhdin, A. Neuberger, Y. A. Trofimov, N. A. Krylov, V. Sinica,, N. Kupko. V. Vlachova, E. Zakharian, R. G. Efremov, and A. I. Sobo-levsky, Structural mechanism of heat-induced opening of a temperature-sensitive TRP channel. *Nat. Struct. Mol. Biol.* 2021, **28,** 564–572.
32. H. Shimada, T. Kusakizako, T. H. D. Nguyen, T. Nishizawa, T. Hin, M. Tominaga, O. Nureki, The structure of lipid nanodisc-reconstituted TRPV3 reveals the gating mechanism. *Nat Struct Mol Biol.* 2020, **27,** 645-652.
33. F. J. Taberner, A. López-Córdoba, G. Fernández-Ballester Y, Korchev, A. Ferrer-Montiel. The region adjacent to the C-end of the inner gate in transient receptor potential melastatin 8 (TRPM8) channels plays a central role in allosteric channel activation. *J. Biol. Chem.* 2014, **289**, 28579–28594.
34. Y. Yin, S. C. Le, A. L. Hsu, M. J. Borgnia, H-Y. Yang, S-Y Lee. Structural basis of cooling agent and lipid sensing by the cold-activated TRPM8 channel. *Science* 2019, **363**, eaav9334.
35. G. Wang. Ligand-stereoselective allosteric activation of cold-sensing TRPM8 channels by an H-bonded homochiral menthol dimer with head-to-head or head-to-tail. *Chirality*. 2021, **33,** 783-796.

36. M. Pertusa, B. Rivera, A. González, G. Ugarte, R. Madrid. Critical role of the pore domain in the cold response of TRPM8 channels identified by ortholog functional comparison. *J. Biol. Chem.* 2018, **293,** 12454–12471.

Figure legends

Fig. 1. **The grid-like non-covalently interacting mesh network along the PIP_2-dependent gating pathway of closed mTRPM8 without Ca^{2+} bound at 4 °C and pH 8.**

A, The topological grids in the systemic fluidic grid-like mesh network. The cryo-EM structure of one subunit in homotetrameric closed mTRPM8 without Ca^{2+} at 4 °C and pH 8 (PDB ID, 7WRA) was used for the model. Salt bridges, π interactions, and H-bonds between pairing amino acid side chains along the PIP_2-dependent gating pathway from Q675 to F1015 are marked in purple, green, and orange, respectively. The grid sizes required to control the relevant non-covalent interactions were constrained with graph theory and labeled in black. The P855-W994 bridge in the biggest $Grid_{21}$ was highlighted. The calculated total grid sizes and noncovalent interactions are shown in the cyan and black circles, respectively. The dashed purple line is the putative salt bridge at 40 °C**.** **B,** The structure of the biggest $Grid_{21}$ in the S4-S5 liker-S5/TRP-S6 interfaces. **C,** The sequence of the biggest $Grid_{21}$ to control the P855-W994 π interaction in the blue box.

Fig. 2. **The grid-like non-covalently interacting mesh network along the PIP_2-dependent gating pathway of closed mTRPM8 with Ca^{2+} bound at 4 °C and pH 8.**

A, The topological grids in the systemic fluidic grid-like mesh network. The cryo-EM structure of one subunit in homotetrameric closed mTRPM8 with Ca^{2+} bound at 4 °C and pH 8 (PDB ID, 7WRB) was used for the model. Salt bridges, π interactions, and H-bonds between pairing amino acid side chains along the PIP_2-dependent gating pathway from Q675 to F1015 are marked in purple, green, and orange, respectively. The grid sizes required to control the relevant non-covalent interactions were constrained with graph theory and labeled in black. The P855-W994 bridge in the biggest $Grid_{21}$ was highlighted. The calculated total grid sizes and noncovalent interactions are shown in the cyan and black circles, respectively. The dashed purple line is the putative salt bridge at 40 °C**.** **B,** The structure of the biggest $Grid_{21}$ in the S4-S5 liker-S5/TRP-S6 interfaces. **C,** The sequence of the biggest $Grid_{21}$ to control the P855-W994 π interaction in the blue box.

Fig. 3. **The grid-like non-covalently interacting mesh network along the PIP_2-dependent gating pathway of open mTRPM8 with Ca^{2+}, PIP_2, C3 and AITC bound at 20 °C and pH 8.**

A, The topological grids in the systemic fluidic grid-like mesh network. The cryo-EM structure of one subunit in homotetrameric open mTRPM8 with Ca^{2+}, PIP_2, C3 and AITC bound at 20 °C and pH 8 (PDB ID, 8E4L) was used for the model. The pore domain, the S4-S5 linker, the TRP domain, the VSLD and the pre-S1 domain are indicated in black. Salt bridges, π interactions, and H-bonds between pairing amino acid side chains along the PIP_2-dependent gating pathway from Q675 to F1015 are marked in purple, green, and orange, respectively. The grid sizes required to control the relevant non-covalent interactions were constrained with graph theory and labeled in black. The F874-Y908 bridge in the biggest $Grid_{22}$ at about 7°C was highlighted. The calculated total grid sizes and noncovalent interactions are shown in the cyan and black circles, respectively. The dashed line was the primary R885-Y905 cation-π interaction for channel opening below 21 °C. **B,** The structure of the PIP_2 binding site. **C**, The structure of the biggest $Grid_{26}$ in the pore domain. **D,** The sequences of the biggest $Grid_{19}$ and $Grid_{26}$ to control the R885-Y905 and F874-Y908 π interactions in the blue boxes, respectively.

Fig. 4. **Cross-examination of the gating $Grid_8$ in open mTRPM8.**

The cryo-EM structure of one subunit in homotetrameric open mTRPM8 with Ca^{2+}, PIP_2, C3 and AITC bound at 20 °C and pH 8 (PDB ID, 8E4L) was used for the model. **A,** The structure of the gating $Grid_8$ in the VSLD/S4-S5 liker/TRP interfaces. **B,** The H845A mutation could induce the formation of the stimulatory R842-E1004 salt bridge. **C,** The protonation of H845 at pH 6 disrupted the stimulatory H845-E1004 H-bond and E1004-R842 salt bridge.

Fig. 5. The tentative cold switches in the TRPM8 biothermometer.

A, The homo-tetrameric cryo-EM structure of mTRPM8 with (PDB ID, 8E4L) or without (PDB ID, 7WRA) Ca^{2+}, PIP2, C3 and AITC bound at 20 °C or 4 °C and pH 8 was used for the model of the open or closed state, respectively. For a convenient view, only two opposite subunits are shown. The dashed rectangle is the membrane area. The biggest $Grid_{21}$ acts as a cold switch for PIP_2–binding to initiate TRPM8 opening at the calculated T_m of 22 °C. This open state was further stabilized by the biggest $Grid_{26}$ at the calulated T_m of 7 °C (Table 1).

Figures

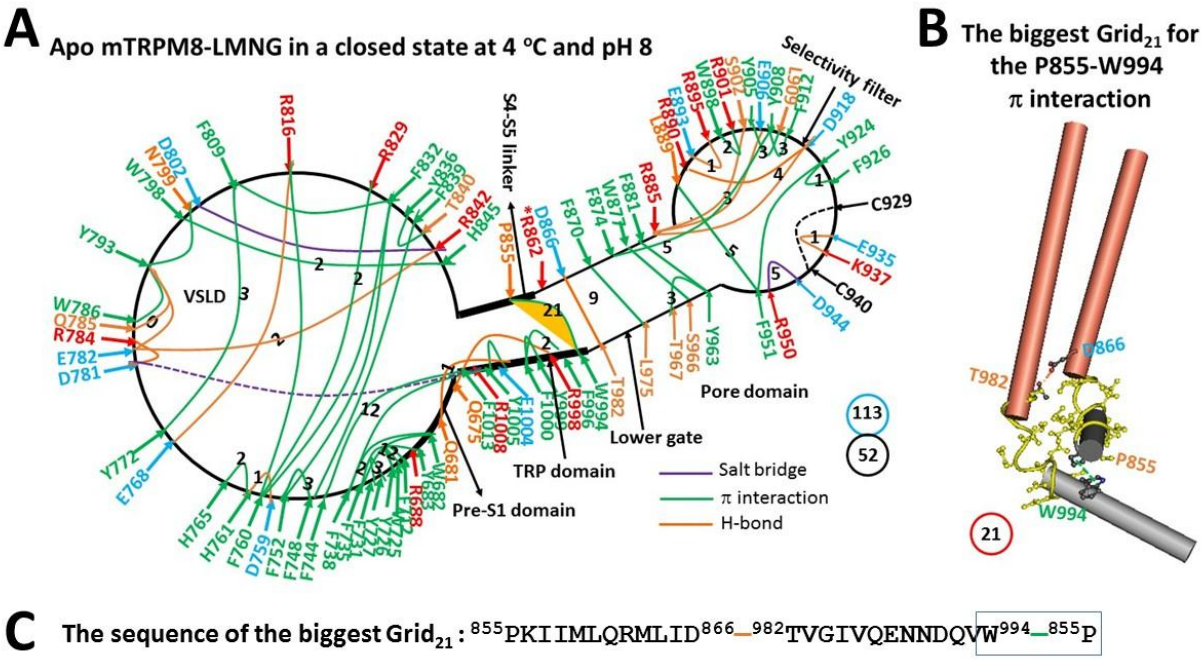

Fig. 1

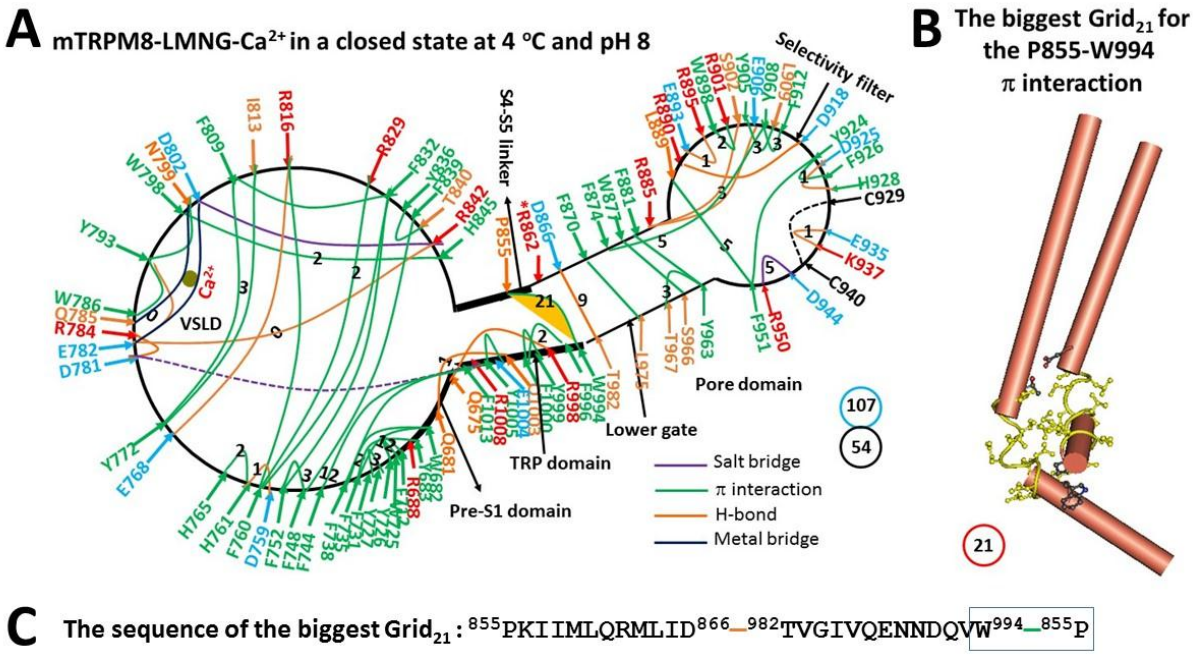

Fig. 2

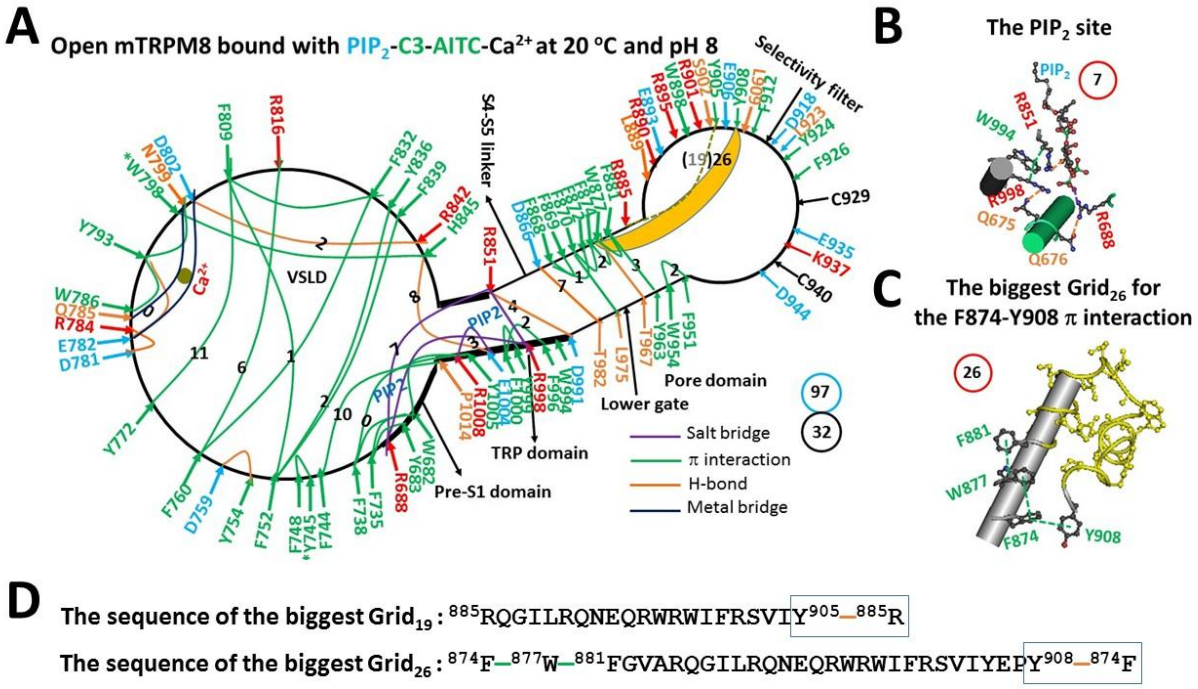
A
Open mTRPM8 bound with PIP2-C3-AITC-Ca2+ at 20 °C and pH 8
Selectivity filter
S4-S5 linker
VSLD
Pore domain
Lower gate
TRP domain
Pre-S1 domain
Salt bridge
π interaction
H-bond
Metal bridge
B
The PIP2 site
C
The biggest Grid26 for the F874-Y908 π interaction
D
The sequence of the biggest Grid19 : 885RQGILRQNEQRWRWIFRSVIY905–885R
The sequence of the biggest Grid26 : 874F–877W–881FGVARQGILRQNEQRWRWIFRSVIYEPY908–874F

Fig. 3

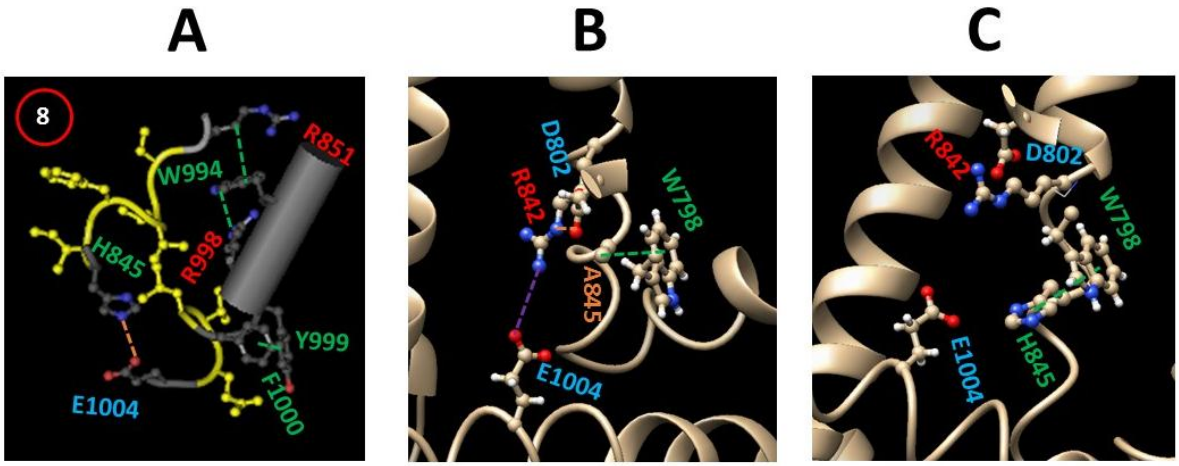
A
B
C
8
R851
W994
H845
R998
Y999
E1004
F1000
D802
R842
W798
A845
E1004
R842
D802
W798
E1004
H845

Fig. 4

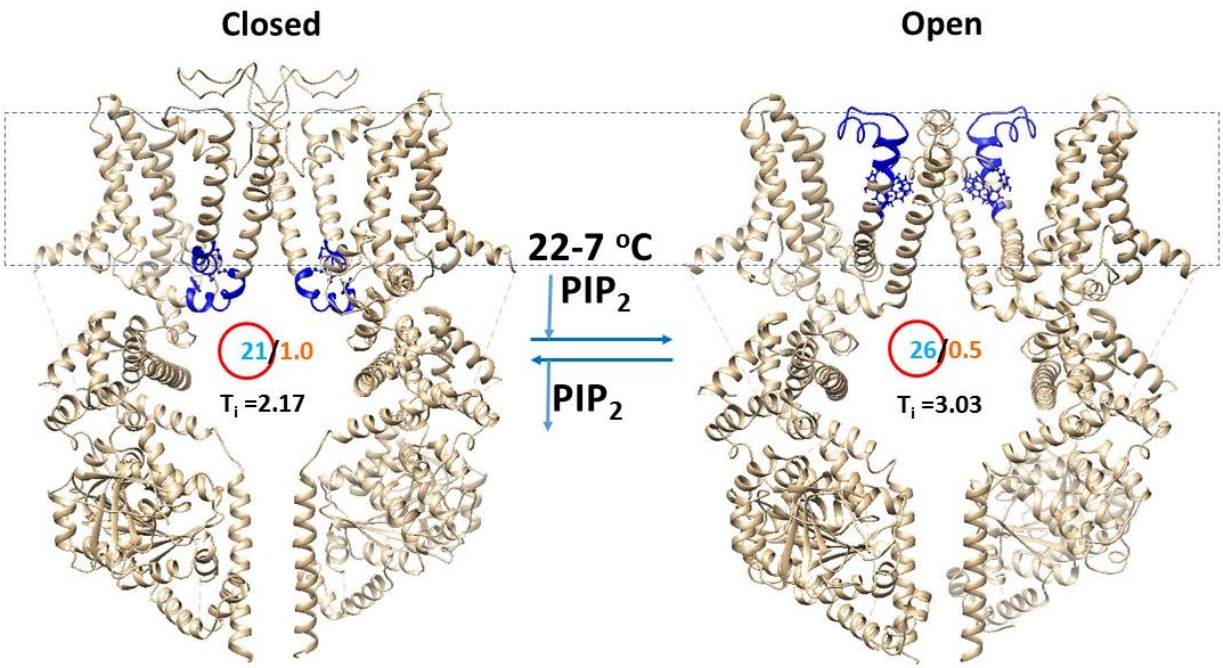

Fig. 5